Dendritic bistability increases the robustness of persistent neural activity in a model oculomotor neural integrator

M.S. Goldman, J.H. Levine, H.S. Seung

ABSTRACT:

Short-term memory is often correlated with persistent changes in neuronal firing rates in response to transient inputs. We model the persistent maintenance of an analog eye position signal by an oculomotor neural integrator receiving transient eye movement commands. Previous models of this network rely on precisely tuned positive feedback with <1% tolerance to mistuning. We show analytically how using neurons with multiple bistable dendritic compartments can enhance the robustness of eye fixations to mistuning while reproducing the observed linear relationship between neuronal firing rates and eye position. We calculate the network dynamics and tolerance to mistuning.

The oculomotor neural integrator is a brain area that converts (integrates) velocity-coded eye movement commands into signals that control eye position. Integrator neurons display persistent firing at a rate proportional to eye position long after the eye movement command has terminated. Thus, the integrator neurons are said to maintain a 'memory of eye position'.

Experimental studies of the goldfish oculomotor neural integrator display several prominent features: (1) persistent firing at a rate that is threshold linearly related to eye position, with different thresholds and slopes for different neurons (Aksay et al., 2000); (2) linear firing rate vs. somatic current injection relationship (Aksay et al., 2001); (3) exponential decay or growth of firing rates when the network is strongly perturbed (Major et al., submitted); and (4) robustness to small perturbations. Previous network models of this system based on positive feedback have been able to capture the first three features above (Seung et al., 2000). The basic idea of these models is that, in the absence of recurrent feedback, the firing rate of a neuron will rapidly decay to a low value. Precisely tuned feedback from neighboring neurons can balance this intrinsic decay to maintain the firing rate of the neuron at an arbitrary constant level. However, to achieve experimentally observed times of stable fixation, these models require the recurrent feedback connections to be tuned to a precision of less than 1%. Recently, neuronal bistability has been proposed as a mechanism to increase the robustness of persistent firing in the integrator (Koulakov et al., submitted). Bistability has been shown to stabilize persistent activity in models of working memory (Lisman et al., 1998; Camperi and Wang, 1998). However, it remains unclear how neuronal bistability can be consistent with the observed linear relationship of firing rate and eye position.

Here, we present an analytic model of the integrator that uses positive feedback mediated by bistable dendritic compartments. Integrator neurons have extensive dendritic processes (Aksay et al., 2000) that could contain many functionally separate compartments. Plateau potentials have been observed in the dendrites of neurons and may be mediated by voltage-dependent NMDA receptors and/or calcium channels (Reuvini et al., 1993; Yuste et al., 1994; Schiller et al., 2000). The linear relationship between firing rate and eye position in our model is achieved by summing the currents from multiple dendritic compartments that turn on at different eye positions.

We consider a network of N neurons that controls the eye position E in the positive half of its range ($E>0$). Each neuron has N dendrites, each of which receives recurrent input from one of the N neurons in the network (Fig. 1A). We assume the current produced by each of the dendrites onto which neuron j projects has identical dynamics that are independent of the somatic firing rate. The contribution of the dendrite receiving input from the j^{th} neuron to the firing rate r_i of the i^{th} neuron is given by $\xi_i \eta_j D_j(t)$, where $D_j(t)$ varies from 0 to 1 and describes the dynamics of the dendritic activation for all dendrites to which neuron j projects. η_j gives the uniform weight of activation of all dendrites to which neuron j projects. ξ_i can be interpreted either as the strength of coupling of neuron i's dendrites to its soma or as the slope of its firing rate vs. somatic current injection relationship. The above arrangement reduces the dynamics of the network to a one-dimensional manifold parameterized by the quantity $\hat{E} \equiv \sum_{i=1}^{N} \eta_i D_i$ (see below).

The firing rate r_i is given by a thresholded sum of contributions from eye movement command inputs $r_{com,i}$, tonic background inputs $r_{ton,i}$, and recurrent input from the other integrator neurons $r_{rec,i} = \xi_i \sum_{j=1}^{N} \eta_j D_j = \xi_i \hat{E}$,

$$r_i = [\xi_i \hat{E} + r_{ton,i} + r_{com,i}]_+ , \quad (1)$$

where $[\ ]_+$ denotes thresholding (Fig. 1B). Because each of the firing rates depends linearly on $\hat{E}$, we interpret this quantity as the neural representation of eye position.

We model the dendrites as having plateau behavior defined by a bistable steady-state function $h(r)$ (Fig. 1C): When the input exceeds a rate r_{on}, the dendrite turns 'on' ($h(r)$=1) and when the input drops below a rate r_{off}, the dendrite turns 'off' ($h(r)$=0). The approach to the 'on' and 'off' states is exponential with time constant τ_{rec},

$$\tau_{rec} \frac{dD_i}{dt} = -D_i + h(r_i) \quad (2)$$

Multiplying equation (2) by η_i and summing over i gives the dynamics of $\hat{E}$,

$$\tau_{rec} \frac{d\hat{E}}{dt} = -\hat{E} + \sum_{i=1}^{N} \eta_i h(\xi_i \hat{E} + r_{ton,i} + r_{com,i}) . \quad (3)$$

The eye velocity $d\hat{E}/dt$ can be determined graphically by considering the difference between the decay term $\hat{E}$ and the summed input term $\sum_{i=1}^{N} \eta_i h(\xi_i \hat{E} + r_{ton,i} + r_{com,i})$ (Figs. 2A-C). For $r_{com,i}$=0, perfect fixations occur when the 45° line defined by $\hat{E}$ lies within the 'band' of stacked hysteretic rectangles defined by the summed input (Fig. 2A). These hysteretic rectangles have shapes and locations determined by the parameters r_{on}, r_{off}, $r_{ton,i}$, ξ_i, and η_i (Fig. 2A). Tuning these parameters can give various shapes of the 'hysteretic band' of summed input.

The width of the hysteretic band determines the robustness of fixations to perturbations of the model parameters. In the absence of hysteresis, small mistuning of the network leads to rapid growth or decay of the firing rates and eye position (Fig. 3A). With hysteresis, significant mistuning can be tolerated with no loss of fixations (Fig. 3B). For the constant couplings illustrated in Figure 2, stable fixations at all eye positions can be maintained over a fractional range of the coupling parameter ξ equal to (up to corrections of $O(\frac{1}{N})$)

$$\frac{\Delta\xi}{\xi^*} = \frac{(r_{on} - r_{off})/\xi^*}{\hat{E}_{max}} , \quad (4)$$

where $\xi^* = \frac{r_{on} + r_{off}}{2\hat{E}_{max}}$ is the value of ξ that centers the hysteretic band around the 45° line (Fig. 2A). The numerator above is the width of the hysteretic band for ξ=ξ^*. Thus, the tolerance to mistuning in this case is given by the width of the tuned band as a fraction of the maximal eye position signal.

Large mistuning of the network leads to either decay to (when feedback is too weak, Fig. 2B) or growth from (when feedback is too large, Fig. 2C) a null eye position $\hat{E}_{null}$ determined by the intersection of the band and the 45° line. When the left or right side of the hysteretic band is linear, the decay or growth (respectively) of eye position is exponential with time constant τ_{decay} or τ_{growth} and can be calculated from the slope of the respective side of the band. For the constant couplings illustrated in Figs. 2B and 2C, $\tau_{decay} = \tau_{growth} = \tau/(1 - \frac{\xi}{\xi^*})$.

We have also conducted simulations of the network in response to head velocity commands involved in the vestibuloocular reflex. We are presently building a biophysically realistic version of the model using heterogeneous synaptic weights and conductance-based

dendritic compartments (Fig. 4). We expect to have simulation results ready in time for the meeting.

REFERENCES:

Aksay E, Baker R, Seung HS, Tank DW (2000) Anatomy and discharge properties of pre-motor neurons in the goldfish medulla that have eye-position signals during fixations. *J Neurophysiol* 84:1035-49.

Aksay E, Gamkrelidze G, Seung HS, Baker R, Tank DW (2001) In vivo intracellular recording and perturbation of persistent activity in a neural integrator. *Nat Neurosci* 2:184-93.

Booth V, Rinzel J (1995) A minimal, compartmental model for a dendritic origin of bistability of motoneuron firing patterns. *J Comput Neurosci* 2:299-312.

Camperi M, Wang XJ (1998) A model of visuospatial working memory in prefrontal cortex: recurrent network and cellular bistability. *J Comput Neurosci* 5:383-405.

Koulakov AA, Kepecs A, Raghavachari S, Lisman JE, submitted.

Lisman JE, Fellous JM, Wang XJ (1998) A role for NMDA-receptor channels in working memory. *Nat Neurosci* 1:273-5.

Major G, Baker R, Mensh B, Aksay E, Seung HS, Tank DW, Plasticity of oculomotor neural integrator dynamics: tuning persistent activity, submitted.

Reuveni I, Friedman A, Amitai Y, Gutnick MJ (1993) Stepwise repolarization from Ca2+ plateaus in neocortical pyramidal cells: evidence for nonhomogeneous distribution of HVA Ca2+ channels in dendrites. *J Neurosci* 13:4609-21.

Schiller J, Major G, Koester HJ, Schiller Y (2000) NMDA spikes in basal dendrites of cortical pyramidal neurons. *Nature* 404:285-9.

Seung HS, Lee DD, Reis BY, Tank DW (2000) Stability of the memory of eye position in a recurrent network of conductance-based model neurons. *Neuron* 26:259-71.

Yuste R, Gutnick MJ, Saar D, Delaney KR, Tank DW (1994) Ca2+ accumulations in dendrites of neocortical pyramidal neurons: an apical band and evidence for two functional compartments. *Neuron* 13:23-43.

FIGURE CAPTIONS:

Figure 1: Network structure. *A*, Compartmental structure and network connectivity. Each neuron in the network couples to a single dendritic compartment of every neuron. The contribution of neuron *j* on the firing of neuron *i* is assumed to be of outer product form $\xi_i \eta_j D_j(t)$ where $D_j(t)$ describes the dynamics of dendritic activation (see text). *B*, Steady-state ($r_{com,i}$=0) firing rate of each neuron *i* is a threshold linear function of $\hat{E} \equiv \sum_{i=1}^{N} \eta_i D_i$ with slope ξ_i and threshold $-r_{ton,i} / \xi_i$. We interpret $\hat{E}$ as the network's representation of eye position. *C*, Hysteretic steady-state activation of each dendrite in response to input of rate *r*.

Figure 2: Graphical representation of network dynamics in the absence of velocity command input ($r_{com,i}$=0) . Individual rectangles give the steady state activation of the dendrites to which neuron *i* projects, weighted by η_i, as a function of $\hat{E}_i$. The rectangles have height η_i, width $(r_{on} - r_{off}) / \xi_i$, turn on at $(r_{on} - r_{ton,i}) / \xi_i$, and turn off at $(r_{off} - r_{ton,i}) / \xi_i$. The eye velocity $d\hat{E}/dt$ at any eye position $\hat{E}$ is proportional to the difference between the thin line representing the sum of these weighted steady-state activations and the bold line representing $\hat{E}$. *A*, Network tuned to have stable fixations over the entire range of eye positions and to be equally robust to positive and negative perturbations in the firing rate of each neuron (ξ=ξ^*). *B*, Network mistuned to decay. The network maintains steady fixations for values of $\hat{E}$ less than the intersection $\hat{E}_{null}$ of the thin and bold lines and decays to this value for greater initial values of $\hat{E}$. *C*, Network mistuned to instability. The network maintains steady fixations for values of $\hat{E}$ less than $\hat{E}_{null}$ and grows unstably to $\hat{E}_{max}$ for greater initial values of $\hat{E}$. Diagrams correspond to couplings $\xi_i = \xi$ and $\eta_i = \hat{E}_{max}/N$, and equally spaced tonic inputs $r_{ton,i} = \frac{1}{2}(r_{on} + r_{off})[1 - (i - \frac{1}{2}) / N]$.

Figure 3: Performance of a mistuned network with and without dendritic hysteresis. A, In the absence of dendritic hysteresis (r_{on}=r_{off}=1 Hz), $\hat{E}$ (*top*) and the firing rates of each neuron (one example, *bottom*) exhibit rapid decay for small (10%) mistuning of couplings. B, With dendritic hysteresis (r_{on}=1 Hz, r_{off}=9.4 Hz, $\Delta\xi/\xi^*$=21%), $\hat{E}$ (*top*) and the firing rates of each neuron (one example, *bottom*) maintain steady fixations in the presence of 10% mistuning of couplings. The overshoots in rate reflect the constant burst input $r_{com,i}$=±20 Hz. The subsequent undershoots are an artifact of the slow activation of the dendritic plateaus in this model (equation (2)). Parameters are as in Figure 2 with τ_{rec} = 100 ms and N=100, and $\hat{E}_{max}$=50°. Mistuning was achieved by setting ξ=0.9ξ^*.

Figure 4: Behavior of a model bistable dendrite adapted from Booth and Rinzel (1995). Voltage of the dendrite as an injected current is ramped up (*bottom branch*) and then down (*top branch*). Plateau behavior is generated by voltage-gated Ca^{++} channels.

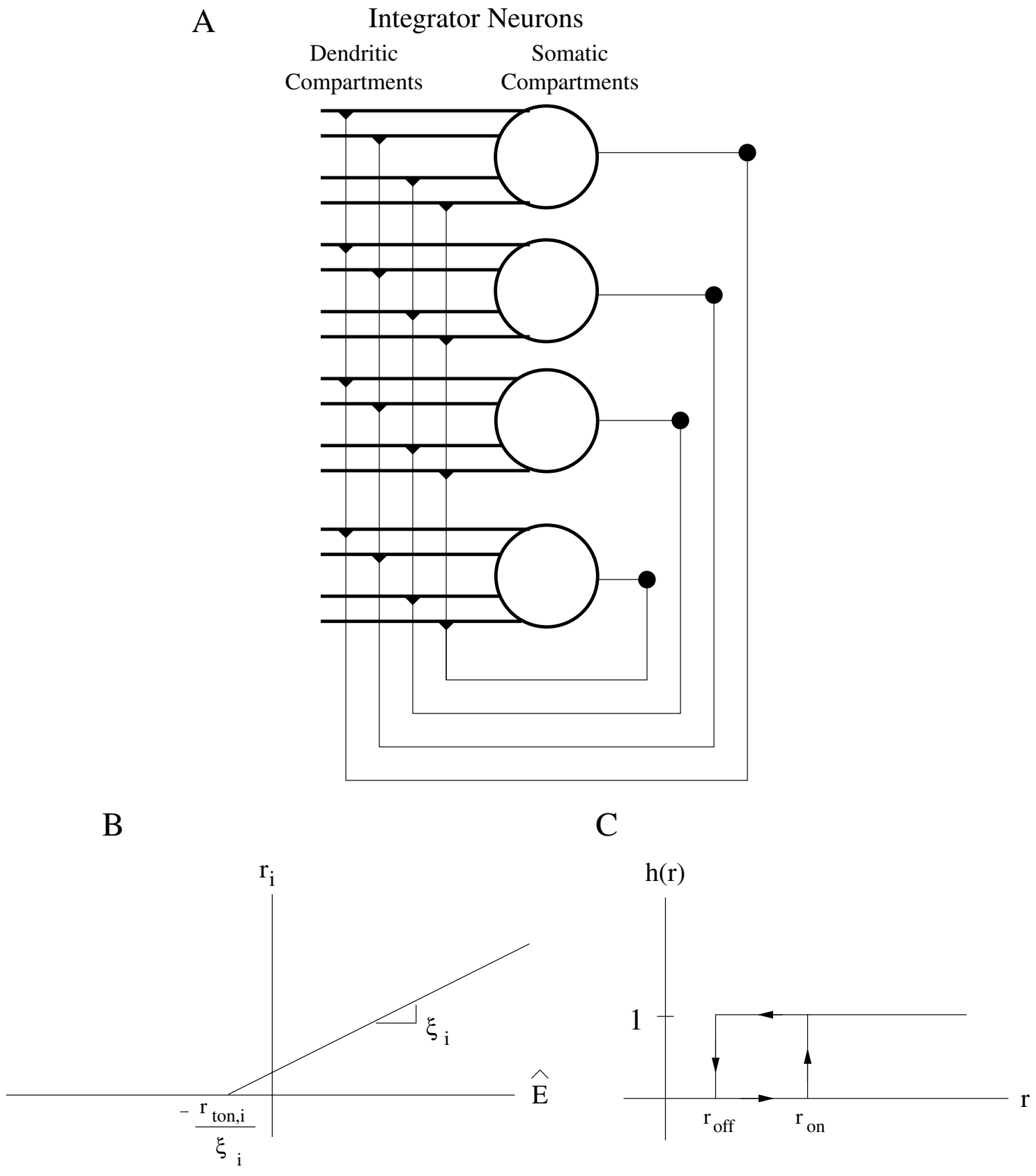
A
Integrator Neurons
Dendritic Compartments
Somatic Compartments
B
r_i
ξ_i
$\hat{E}$
$-\frac{r_{ton,i}}{\xi_i}$
Somatic Rate Response
C
h(r)
1
r_{off}
r_{on}
r
Single Dendrite Response

Figure 1

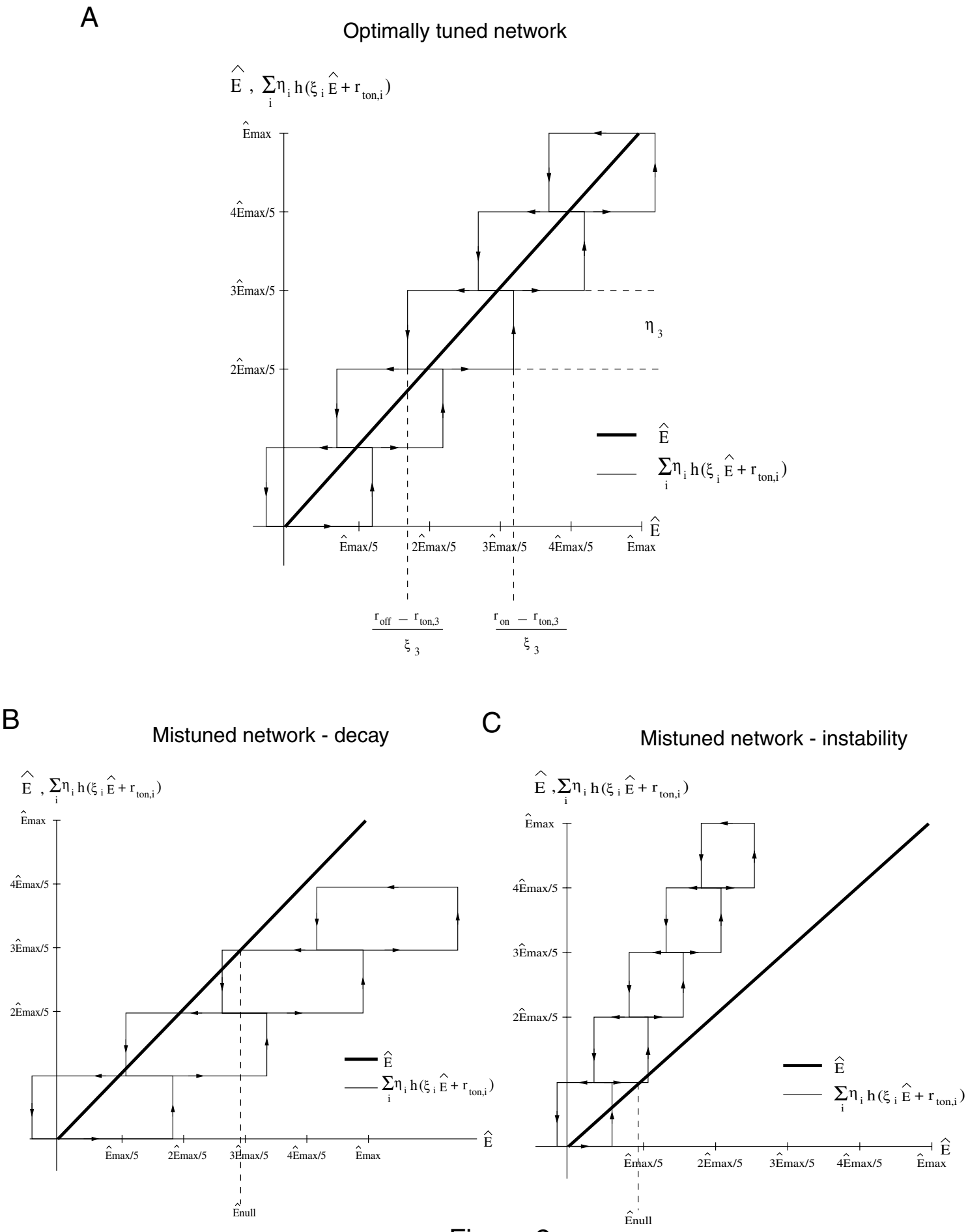
A
Optimally tuned network
$\hat{E}$, $\sum_i \eta_i h(\xi_i \hat{E} + r_{ton,i})$
$\hat{E}max$
$4\hat{E}max/5$
$3\hat{E}max/5$
$2\hat{E}max/5$
η_3
$\hat{E}$
$\sum_i \eta_i h(\xi_i \hat{E} + r_{ton,i})$
$\hat{E}max/5$
$2\hat{E}max/5$
$3\hat{E}max/5$
$4\hat{E}max/5$
$\hat{E}max$
$\hat{E}$
$\frac{r_{off} - r_{ton,3}}{\xi_3}$
$\frac{r_{on} - r_{ton,3}}{\xi_3}$
B
Mistuned network - decay
$\hat{E}$, $\sum_i \eta_i h(\xi_i \hat{E} + r_{ton,i})$
$\hat{E}max$
$4\hat{E}max/5$
$3\hat{E}max/5$
$2\hat{E}max/5$
$\hat{E}$
$\sum_i \eta_i h(\xi_i \hat{E} + r_{ton,i})$
$\hat{E}max/5$
$2\hat{E}max/5$
$3\hat{E}max/5$
$4\hat{E}max/5$
$\hat{E}max$
$\hat{E}$
$\hat{E}null$
C
Mistuned network - instability
$\hat{E}$, $\sum_i \eta_i h(\xi_i \hat{E} + r_{ton,i})$
$\hat{E}max$
$4\hat{E}max/5$
$3\hat{E}max/5$
$2\hat{E}max/5$
$\hat{E}$
$\sum_i \eta_i h(\xi_i \hat{E} + r_{ton,i})$
$\hat{E}max/5$
$2\hat{E}max/5$
$3\hat{E}max/5$
$4\hat{E}max/5$
$\hat{E}max$
$\hat{E}$
$\hat{E}null$

Figure 2

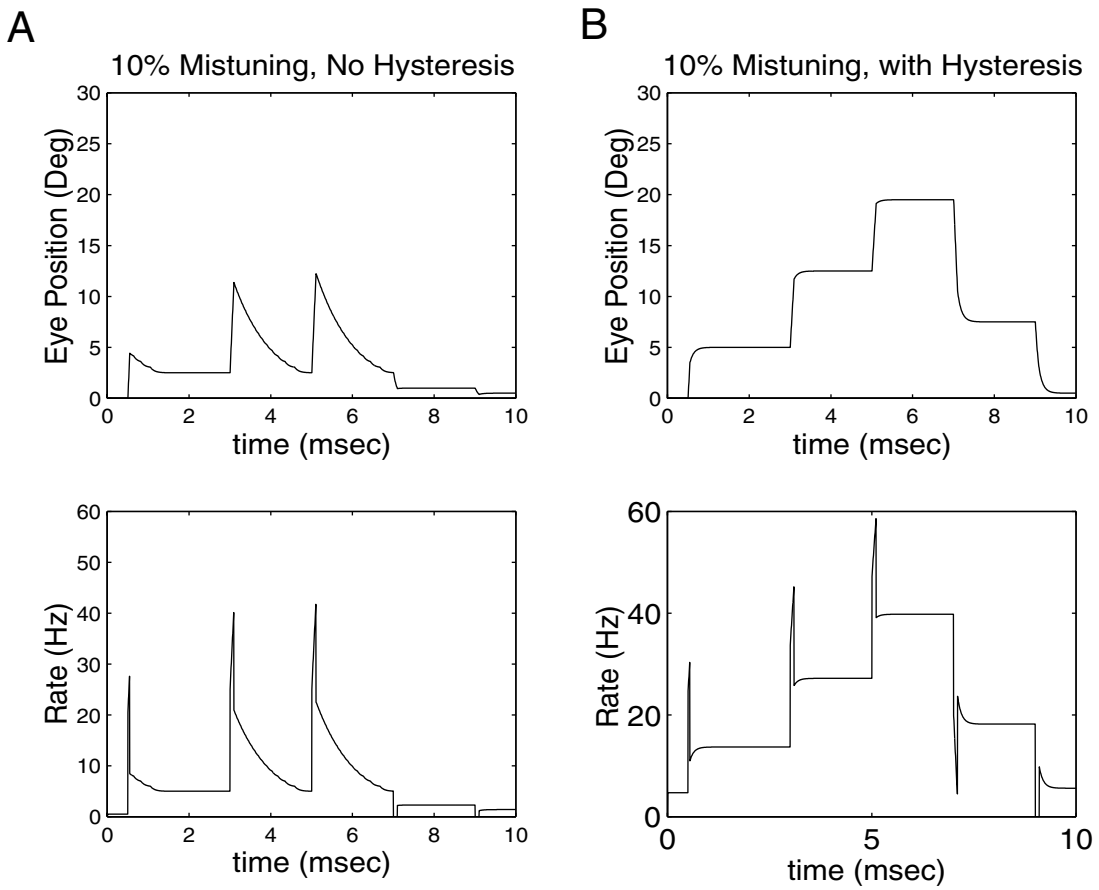

Figure 3

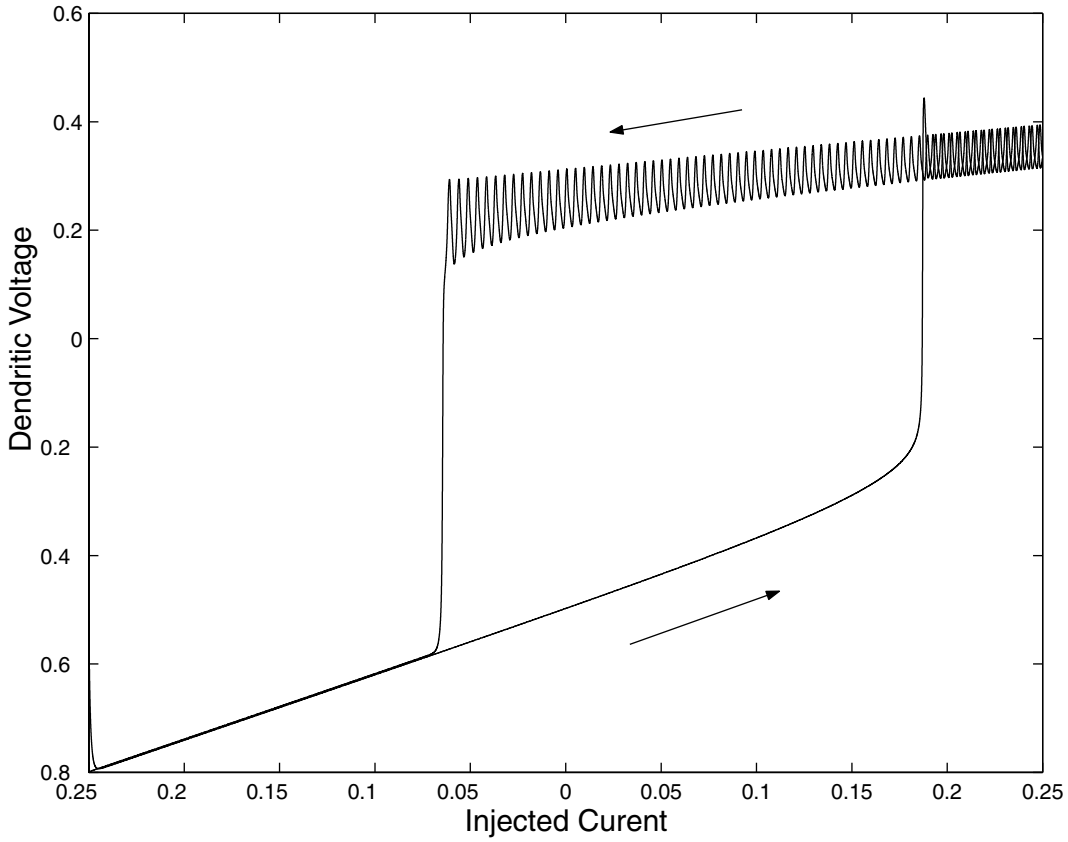

Figure 4